Proceedings of the 1999 IEEE International Conference on Robotics & Automation, May 1999, Detroit, Michigan

Interaction with a Realtime Dynamic Environment Simulation using a Magnetic Levitation Haptic Interface Device

Peter J. Berkelman and Ralph L. Hollis
The Robotics Institute
Carnegie Mellon University
Pittsburgh, PA 15213

David Baraff
Pixar Animation Studios
Richmond CA, 94804

Abstract

A high performance six degree-of-freedom magnetic levitation haptic interface device has been integrated with a physically-based dynamic rigid-body simulation to enable realistic user interaction in real time with a 3-D dynamic virtual environment. The user grasps the levitated handle of the device to manipulate a virtual tool in the simulated environment and feels its force and motion response as it contacts and interacts with other objects in the simulation.

The physical simulation and the magnetic levitation controller execute independently on separate processors. The position and orientation of the virtual tool in the simulation and the levitated handle of the maglev device are exchanged at each update of the simulation. The position and orientation data from each system act as impedance control setpoints for the other, with position error and velocity feedback on each system acting as virtual coupling between the two systems. The setpoints from the simulation are interpolated by the controller at the faster device control rate so that the user feels smooth sliding contacts without chattering due to the slower updates of the simulation. The simple feedback coupling between the two systems enables the overall stiffness and stability of the combined system to be tuned easily and provides realistic haptic user interaction. Sample task simulation environments have been programmed to demonstrate the effectiveness of the haptic interaction system.

1 Introduction

Haptic refers to the tactile and kinesthetic sensing modalities of the hand. The aim of the work described here is to provide high fidelity tool-based haptic interaction with a dynamic simulated rigid-body environment so that a user can grasp a tool handle on the haptic interface device to interact in real time with simulated manual task environments while feeling the detailed reaction forces of the tool in the simulation due to solid contacts, friction, and texture. Magnetic levitation devices are well suited for haptic interaction due to simple control dynamics, full 6-DOF motion with one moving part, high control bandwidths, and the absence of actuator nonlinearities such as backlash and hysteresis. Potential applications of haptic interface technology include prototyping, simulation, training, and teleoperation in areas such as medical, CAD, machine or vehicle operation[1, 2, 3].

A graphic display of the simulated environment is also generated during haptic interaction. A simple coupling method provides a general way to interface a haptic interface device with any realtime simulation to provide the user with realistic, stable interaction with a simulated environment model of a haptic task.

Lorentz force magnetic levitation devices have previously been developed by Hollis and Salcudean [4, 5]. The new device described here has a larger range of motion and was designed specifically for haptic interaction instead of as a fine motion robot wrist. Haptic interaction for solid contacts and friction has been developed using previous magnetic levitation devices by Salcudean and Berkelman [6, 7].

Colgate *et al.* first proposed using a virtual coupling between a simulation and a haptic display to simplify design and ensure stability [8] and Adams and Hannaford generalized the idea and analyzed its stability conditions [9]. The use of interpolated, locally updated intermediate representations to interface haptic devices with simulations at a slower update rate has been developed by Adachi, Mark *et al.*, and Vedula [10, 11, 12], primarily for point force interactions rather than for 6-DOF rigid-body interaction.

2 Maglev Haptic Interface Device

The use of noncontact actuation and sensing with a single lightweight moving part results in control bandwidths and position resolution that would be very difficult to achieve with any conventional 6-DOF force feedback linkage mechanism. The actuation forces of the magnetic levitation device are caused by the Lorentz force generated on wire coils carrying electric current in a magnetic field. Six Lorentz force actuators arranged about the levitated bowl enable forces and torques to be generated in all directions. Three sensor assemblies focus light from LEDs on the levitated

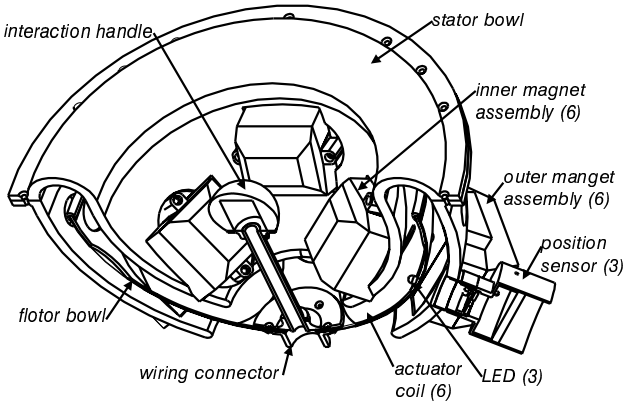

Figure 1: Cutaway View of the Maglev Haptic Device

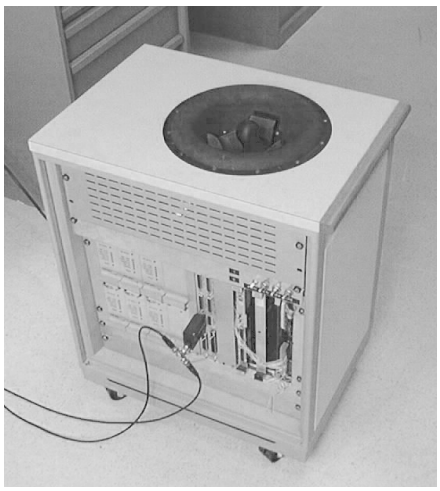

Figure 2: Haptic Interface Device Enclosure

bowl through lenses onto fixed planar position sensing photodiodes to provide noncontact position sensing. A cutaway schematic of the magnetic levitation device showing the fixed stator with magnet and sensor assemblies and the levitated flotor with coils, LEDs, and the interaction handle is given in Fig. 1. Additional details of the device design are described in a design paper[13].

Our maglev device and its amplifiers, controller, and power supplies are contained in a single desktop-height cabinet shown in Fig. 2. The device cabinet can be easily positioned next to a desk for user operation with a graphical display, as in Fig. 3. The interaction handle of the device is at desktop level and the top rim of the magnet stator bowl mounted into the top of the cabinet so that the user can manipulate the handle with the fingertips while resting his or her wrist on the rounded rim of the permanent magnet housing.

The range of motion of the levitated handle is 25 mm in translation and 15-20° in rotation in all directions to provide a comfortable fingertip motion range. For small motion amplitudes, the ± 3 dB attenuation position control bandwidth of the magnetic levitation device is 100 Hz or greater for all axes. The closed-loop position control and sensing resolution of the device is 5-10 μm throughout its motion range. The maximum sample rate of the present 68060 control processor is 1.4 kHz. The peak forces and torques attainable are limited to 50 N and 6 Nm by the current amplifiers in use. The translational stiffness range is 0.005 N/mm to 25.0 N/mm. More results are given in a dynamic performance paper [14].

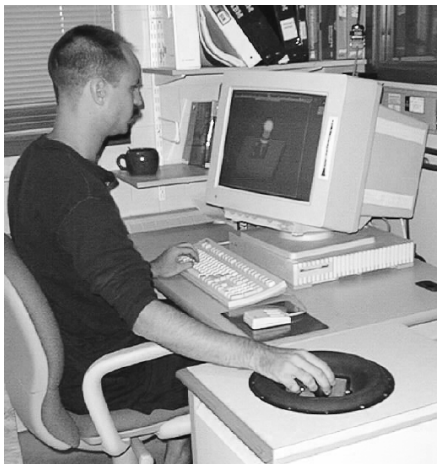

Figure 3: Using the Haptic Interface Device with a Graphics Display

3 Physical Simulation

The CORIOLIS$^{\text{tm}}$ 3-D physically-based dynamic simulation package developed by Baraff, an extension of the 2-D simulation described in [15], is used for the interactive simulation. This package calculates forces and motions of rigid bodies in space due to Newtonian mechanics, motion constraints, collisions, and friction quickly and efficiently.

The Newtonian free rigid-body dynamic state equations given below are integrated for each free body in the simulation:

$$\frac{d}{dt}\begin{pmatrix} \boldsymbol{x}(t) \\ \boldsymbol{R}(t) \\ \boldsymbol{P}(t) \\ \boldsymbol{L}(t) \end{pmatrix} = \begin{pmatrix} \boldsymbol{v}(t) \\ \boldsymbol{\omega}(t)\boldsymbol{R}(t) \\ \boldsymbol{F}(t) \\ \boldsymbol{\tau}(t) \end{pmatrix},$$

$$\boldsymbol{v}(t) = \frac{\boldsymbol{P}(t)}{M}, \quad \boldsymbol{\omega}(t) = \boldsymbol{I}(t)\boldsymbol{L}(t),$$

$$\boldsymbol{I}(t) = \boldsymbol{R}(t)\boldsymbol{I}_{body}\boldsymbol{R}(t)^T.$$

with position $\boldsymbol{x}$, rotation matrix $\boldsymbol{R}$, momentum $\boldsymbol{P}$, angular momentum $\boldsymbol{L}$, velocity $\boldsymbol{v}$, angular velocity $\boldsymbol{\omega}$, force $\boldsymbol{F}$, and torque $\boldsymbol{\tau}$. Body mass M is constant and inertia $\boldsymbol{I}$ is a coordinate transform of constant inertia matrix $\boldsymbol{I}_{body}$.

When contact is detected, the necessary surface forces to prevent interpenetration are computed and introduced into the simulation. For collisions, the impulsive forces and accelerations are instantaneous so integration must be restarted with new initial conditions since differential equation integration methods assume continuous dynamics. Simulated objects are perfectly rigid and non-interpenetrating and bounding boxes are used for fast collision detection.

The simulation was tuned to run as fast as possible for realistic realtime interaction. The midpoint or second-order Runge-Kutta integration method was selected for speed and simplicity. A 100 Hz update rate was achieved for simulations with up to 10 polyhedral objects of 10 vertices or less on an SGI Indigo 2 workstation. If the multiple rigid body contact states are sufficiently complex, such as when a chain of several objects collides nearly simultaneously, the simulation update rate may occasionally slow down for one or two frames.

The 3-D rendered graphics display is updated asynchronously in the background after the simulation dynamics are updated by an interval timer signal handler. The resulting frame rate of the graphics display is typically 15-30 Hz, depending on the complexity of the simulation and any other processes executing on the workstation.

4 Coupled Simulation and Control

The simulation and the device controller can each operate independently and communicate using TCP/IP sockets over a standard Ethernet network. A schematic representation of the intercommunication between the device, controller, simulation, and graphical display systems is shown in Fig. 4.

Interactive simulations have been implemented on the local control processor but they are limited to static environments with fewer than 10 to 15 total vertices in the models of the tool and its environment. The present control processor is not sufficiently fast to perform dynamic simulation and collision detection on multiple moving objects while calculating the sensor kinematics and feedback control at a rate sufficient for stable stiff contacts.

The virtual coupling between the realtime simulation and the maglev haptic device controller as proposed by Colgate [8] is shown in Fig. 5. In our implementation, the position and orientation vector of each

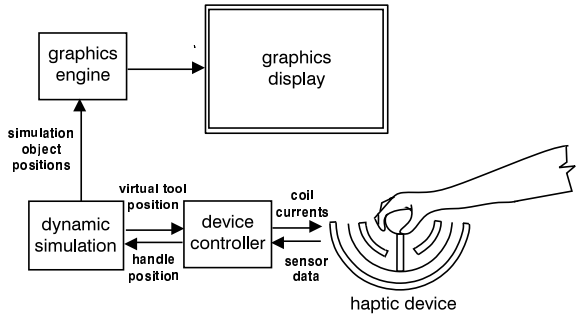

Figure 4: Haptic and Visual Interface System

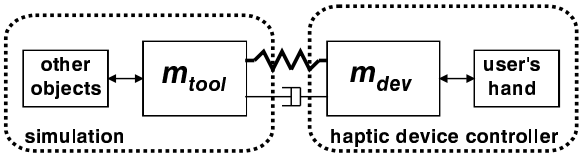

Figure 5: Virtual Coupling of Simulation and Device

system is periodically sent to the other system to act as its control setpoint. The stability and responsiveness of the simulation and device can be set by the spring and damper gains of the coupling as seen from either side. The generated forces on the maglev haptic device $\boldsymbol{f}_{dev}$ and the virtual tool in the simulation $\boldsymbol{f}_{tool}$ are given by:

$$\boldsymbol{f}_{dev} = \boldsymbol{f}_g + \boldsymbol{K}_p(\boldsymbol{x}_{tool} - \boldsymbol{x}_{dev}) + \boldsymbol{K}_v \boldsymbol{r}(\boldsymbol{x}_{dev} - \boldsymbol{x}_{devprev}),$$

$$\boldsymbol{f}_{tool} = \boldsymbol{f}_{other} + \boldsymbol{K}_{spring}(\boldsymbol{x}_{dev} - \boldsymbol{x}_{tool}) + \boldsymbol{K}_{damp}\boldsymbol{v}_{tool}.$$

where $\boldsymbol{f}_g$ is gravity feedforward to reduce the weight of the levitated bowl, $\boldsymbol{K}$ are the coupling gains, $\boldsymbol{r}$ is the control rate of the device, and $\boldsymbol{f}_{other}$ are the forces from the other objects in the simulation. When the virtual tool is not in contact with any other objects in the simulation, force feedback to the device is switched off. Realistic and stable performance for most task simulations has been obtained with the following coupling gains, where $\boldsymbol{K}_{spring}$ and $\boldsymbol{K}_{damp}$ are the gains from the simulation side and $\boldsymbol{K}_p$ and $\boldsymbol{K}_v$ are the maglev device control gains:

Gain	Position	Rotation
$\boldsymbol{K}_{spring}$	100 N/mm	800 Nm/rad
$\boldsymbol{K}_{damp}$	10 N/mm/s	20 Nm/rad/sec
$\boldsymbol{K}_p$	4.0 N/mm	25 Nm/rad
$\boldsymbol{K}_v$	0.1 N/mm/s	0.5 Nm/rad/sec

The time required to send a set of position setpoints from the simulation and receive a reply of setpoints from the control processor is generally approximately 1 ms. The simulated environment takes 10 ms to respond to forces or motions exerted by the user, however, due to its 100 Hz update rate. The response

delay due to this latency is perceived by the user as stickiness or sluggishness in haptic interaction.

Interpolation between the setpoints supplied by the simulation eliminates the jittering or chattering feel experienced by the user during sliding contacts between the simulated tool and other objects. The desired position setpoints $\boldsymbol{x}_{goal}$ on the haptic device controller are interpolated from the last setpoint supplied by the simulation $\boldsymbol{x}_{simnew}$ and the differences between the last setpoint and the previous one $\boldsymbol{x}_{simprev}$:

$$\boldsymbol{x}_{goal} = \boldsymbol{x}_{goal} + \frac{\boldsymbol{x}_{simnew} - \boldsymbol{x}_{simprev}}{T_{avg}}$$

where T_{avg} is the average of the last three simulation time intervals since there are variations due to overruns in the simulation calculations, network traffic, or other delays. This interpolation scheme is a first-order hold since the most recent sample and the slope between samples are used to calculate the interpolated setpoints.

This same method of virtual coupling with interpolated setpoints can be used to add haptic interaction to any realtime simulation that calculates motions due to dynamic forces. Independent operation of the simulation and the haptic device controller significantly simplifies development, testing, and debugging of the integrated system.

Sample tasks have been programmed into the simulation to demonstrate rigid-body haptic tool manipulation. Each of these tasks requires 6-DOF haptic manipulation and feedback and could not be performed with 3 DOF only. The first general task world contains several free polyhedral objects and fixed walls, as pictured in Fig. 6. The user tool is a square scoop with a handle. The scoop can be used to feel, strike, push, pick up, or throw and catch other solid objects in the simulation while the user feels its dynamic response. The second task, shown in Fig. 7, demonstrates the classic peg-in-hole manipulation problem. The world contains only a fixed square hole and the user tool is a peg of a slightly smaller cross-section than the hole. The third task, in Fig. 8, is a variation of the peg-in-hole where the task setup includes a fixed keyhole, a movable bolt, and a key as the haptic user tool. The user can insert the key into the hole and rotate it to slide the bolt sideways.

A one-to-one mapping of the levitated handle position to the virtual tool position in the simulated environment provides sensitive interaction for fine fingertip operations such as insertion, but the user cannot move the tool over larger distances in the simulated environment. Therefore, additional control modes have been added to the haptic user interface to enable the user to operate the haptic tool over arbitrarily large

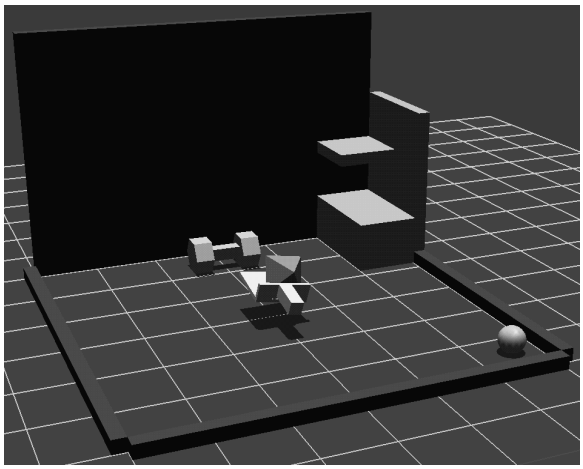

Figure 6: Block Manipulation Task

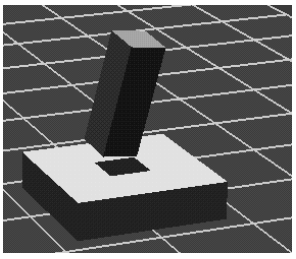

Figure 7: Peg-in-Hole

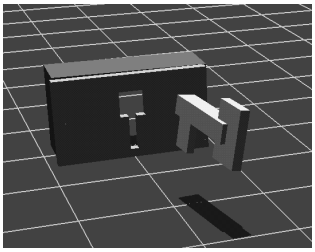

Figure 8: Key and Lock

distances and rotations in the virtual environment in a natural, intuitive way. During interaction the user can change the position scaling factors and zero offsets between the levitated handle and the simulated environment, switch to rate control mode, and move the graphics viewpoint for the simulation display.

The mapping from the actual levitated handle position $\boldsymbol{x}_{device}$ and $\boldsymbol{\Theta}_{device}$ to the simulation setpoint $\boldsymbol{x}_{setp}$ and $\boldsymbol{\Theta}_{setp}$ is given by

$$\boldsymbol{x}_{setp} = \boldsymbol{x}_{offset} + \boldsymbol{x}_{scale}\boldsymbol{x}_{device}, \text{ and}$$

$$\boldsymbol{\Theta}_{setp} = \boldsymbol{\Theta}_{offset} + \boldsymbol{\theta}_{scale}\boldsymbol{\Theta}_{device}.$$

The variable scaling factors $\boldsymbol{x}_{scale}$ and $\boldsymbol{\theta}_{scale}$, and offsets $\mathbf{x}_{offset}$ and $\boldsymbol{\Theta}_{offset}$ for rotation and translation are set by sliders in a graphical user interface control panel. The offsets determine the position and orientation of the virtual tool when the haptic device handle is in the centered position. These offsets can be set so that the full sensitivity and motion range of the haptic interface device can be made available at any point in the simulated environment. The user can easily switch from making large motions across the entire simulation world to fine motions in one spot.

In rate control mode, the position of the haptic device handle determines the velocity instead of the po-

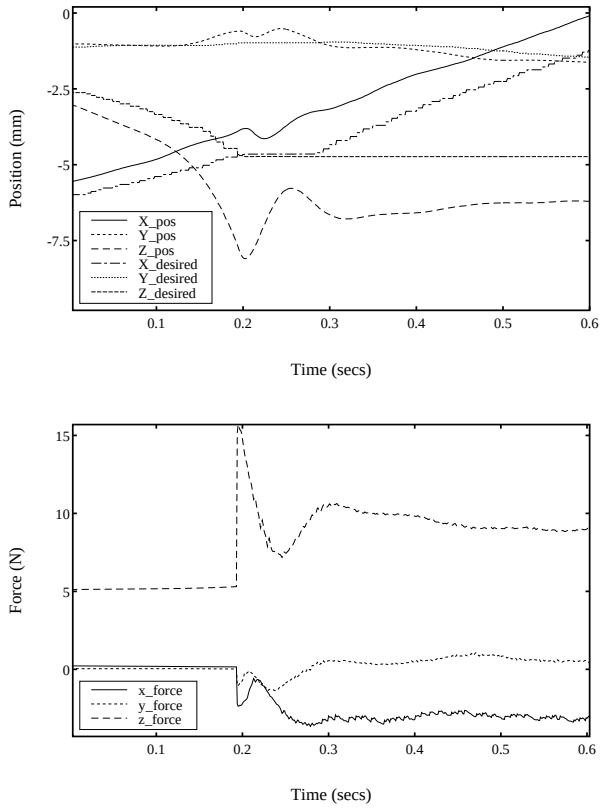

Figure 9: Position and Force Data from Impact and Sliding Motions

sition of the tool in the simulation. Rate control mode can be either manually selected by clicking a button on the user interface control panel window, or automatically invoked as the levitated handle approaches its motion limits.

Viewpoint controls are provided for the user to zoom, rotate, and pan to display areas of interest in the simulated environment. Automatic viewpoint control mode tracks the tool so that the zero offset position of the tool is centered in the display and the major axis of the tool in its zero offset orientation is aligned with the viewing direction.

5 Sample Experimental Results

The data plots in Fig. 9 were obtained from the magnetic levitation controller during typical user interaction with the haptic interface system. Rotation and torque data are not shown. The user brought the virtual scoop of Fig. 6 into contact with the environment floor while moving it in the positive $\boldsymbol{x}$ direction. The data show free tool motion until approximately the 0.2 seconds, then vertical impact and sliding. The desired position setpoints in the controller are obtained from the virtual tool positions in the dynamic simulation.

In unconstrained axes, the desired setpoints lag behind the actual setpoints because there is no force feedback exerted by the system. Due to the slower update rate of the simulation, the desired position setpoint curves have a stair-step appearance. Since objects in the simulation cannot interpenetrate, the $\boldsymbol{z}$ setpoint is pinned to the floor level at -5 mm after impact. There is an inflection in the $\boldsymbol{x}$ position curve after the impact from the user's hand rebounding due to the friction in the simulation.

The force data plot shows the force commands exerted on the flotor by the Lorentz actuators. While the virtual tool is in free space, the user feels no resistance to motions other than the actual inertia and passive eddy current damping in the flotor. No Lorentz forces are generated in the $\boldsymbol{x}, \boldsymbol{y}$ horizontal plane and 5 N are generated upwards in $\boldsymbol{z}$ to partially cancel the weight of the flotor. When the virtual tool in the simulation contacts the floor, the force in $\boldsymbol{y}$ remains close to zero and a negative force in $\boldsymbol{x}$ is generated due to sliding friction modelled in the dynamic simulation. The force in $\boldsymbol{z}$ changes suddenly and rebounds at impact, then settles to support the weight of the flotor and additional disturbance forces from the user's hand.

6 Summary and Conclusions

We have implemented a complete general haptic interface system which demonstrates the effectiveness and practicality of several combined technologies in haptics:

Tool-based haptic interaction using a magnetic levitation device can provide sensitive, high-bandwidth haptic interaction with a dynamic simulation. The virtual spring and damper coupling is a simple yet effective method for coupling a haptic interface device with a simulation to provide realistic, high-performance, 6-DOF haptic interaction. Separation of the simulation and the haptic interface simplifies development and testing and the overall system stiffness and stability can be tuned by adjusting the parameters of the virtual spring and dampers. Setpoint interpolation by the haptic device controller practically eliminates the feel of jitter during sliding contacts caused by the slower update rate of the simulation.

The three tasks set up for the simulation system demonstrate common haptic 6-DOF rigid body tasks that cannot be performed naturally using 3-DOF devices. The added haptic user interface features of rate control mode, variable scaling and offsets, and automatic viewpoint tracking enable the user to navigate in a natural and intuitive manner through an arbitrar-

ily large simulation workspace and also interact with high sensitivity when desired.

7 Planned Work

To further increase the fidelity of haptic interaction, the effects of communication latency and compliance between the simulation and the device must be reduced. To accomplish this, all the virtual tool contact point data will be sent to the device controller from the simulation instead of only its position. The feedback forces generated by the device will be calculated from each contact point rather than simply servoing to the interpolated setpoint.

To add realism and detail to the haptic interaction, surface texture and friction will be modeled on the local control processor and added to the force feedback during sliding contacts. To handle the added computation, the local control processor will be upgraded. Finally, user studies will be carried out to evaluate the effectiveness and ease of use of the haptic interface system.

References

[1] N. Parker, S. Salcudean, and P. Lawrence, "Application of force feedback to heavy duty hydraulic machines," in *IEEE Int'l Conf. on Robotics and Automation*, (Atlanta), pp. 375–381, May 1993.

[2] J. W. Hill, P. S. Green, J. F. Jensen, Y. Gorfu, and A. S. Shah, "Telepresence surgery demonstration system," in *IEEE Int'l Conf. on Robotics and Automation*, (San Diego), pp. 2302–2307, May 1994.

[3] S. Singh, M. Bostrom, D. Popa, and C. Wiley, "Design of an interactive lumbar puncture simulator with tactile feedback," in *IEEE Int'l Conf. on Robotics and Automation*, (San Diego), pp. 1734–1739, May 1994.

[4] R. L. Hollis, S. Salcudean, and A. P. Allan, "A six degree-of-freedom magnetically levitated variable compliance fine motion wrist: design, modeling, and control," *IEEE Transactions on Robotics and Automation*, vol. 7, pp. 320–332, June 1991.

[5] S. Salcudean, N.M. Wong, and R.L. Hollis, "Design and control of a force-reflecting teleoperation system with magnetically levitated master and wrist," *IEEE Transactions on Robotics and Automation*, vol. 11, pp. 844–858, December 1995.

[6] S. Salcudean and T. Vlaar, "On the emulation of stiff walls and static friction with a magnetically levitated input-output device," in *ASME IMECE*, (Chicago), pp. 303–309, November 1994.

[7] P. J. Berkelman, R. L. Hollis, and S. E. Salcudean, "Interacting with virtual environments using a magnetic levitation haptic interface," in *Int'l Conf. on Intelligent Robots and Systems*, (Pittsburgh), August 1995.

[8] J. Colgate, M. Stanley, and J. Brown, "Issues in the haptic display of tool use," in *Int'l Conf. on Intelligent Robots and Systems*, (Pittsburgh), August 1995.

[9] R. Adams and B. Hannaford, "A two-port framework for the design of unconditionally stable haptic interfaces," in *Int'l Conf. on Intelligent Robots and Systems*, (Victoria, B,C.), August 1998.

[10] Y. Adachi, T. Kumano, and K. Ogino, "Intermediate representation for stiff virtual objects," in *Proc. IEEE Virtual Reality Annual Intl. Symposium*, (Research Triangle Park, N.C.), pp. 203–210, March 1995.

[11] W. Mark, S. Randolph, M. Finch, J. V. Werth, and R. Taylor, "Adding force feedback to graphics systems," in *Computer Graphics (Proc. SIGGRAPH)*, pp. 447–452, 1996.

[12] S. Vedula and D. Baraff, "Force feedback in interactive dynamic simulation," in *Proceedings of the First PHANToM User's Group Workshop*, (Dedham, MA), September 1996.

[13] P. J. Berkelman, Z. J. Butler, and R. L. Hollis, "Design of a hemispherical magnetic levitation haptic interface device," in *Proc. of the ASME IMECE Symposium on Haptic Interfaces for Virtual Environment and Teleoperator Systems*, (Atlanta), November 17-22 1996.

[14] P. J. Berkelman and R. L. Hollis, "Dynamic performance of a hemispherical magnetic levitation haptic interface device," in *SPIE Int'l Symposium on Intelligent Systems and Intelligent Manufacturing, SPIE Proc. Vol. 3602*, (Greensburgh, PA), September 1997.

[15] D. Baraff, "Interactive simulation of solid rigid bodies," *IEEE Computer Graphics and Applications*, vol. 15, pp. 63–75, 1995.